
Rotor Vortex Filaments: Living on the Slipstream's Edge

Larry A. Young

January 1997



National Aeronautics and
Space Administration

Rotor Vortex Filaments: Living on the Slipstream's Edge

Larry A. Young, Ames Research Center, Moffett Field, California

January 1997



National Aeronautics and
Space Administration

Ames Research Center
Moffett Field, California 94035-1000

NOMENCLATURE

C_T	Rotor thrust coefficient
dS	Elemental surface (m^2)
dV	Elemental volume (m^3)
g_r	Gravity induced body forces per unit mass (m/sec^2)
$I(x)$	Impulsive force function; x is the argument. Quantifies impulsive force due to vortex-driven flow crossing the slipstream shear layer.
N	Number of rotor blades
n	Normal vector to control surface, used in vorticity conservation surface integrals (positive radially outward)
P	Static pressure (N/m^2)
P_{QSV}	Static pressure component due to quasi-steady vortex-dominated flow (N/m^2)
P_{UNV}	Static pressure component due to flow with unsteady, non-vortex-driven velocity components (dominated instead by large radial and not tangential velocities (N/m^2))
R	Rotor radius (m)
r	Radial coordinate, referenced to the vortex core center (m)
r_c	Vortex core radius initial value, at $t = 0$ (m)
r_o	Outer radial limit of derived stream function solution, where mass transfer across slipstream shear layer ceases (m)
t	Time (sec)
u	Velocity component normal to the vortex core control volume surface element (positive radially outward)
U	Rotor axial-flight freestream velocity (m/sec)
V_T	Rotor tip speed (m/sec)
v	Mean inflow velocity at rotor disk plane (m/sec)

v_i	Rotor slipstream velocity in the far-wake, from momentum theory, $v_i = 2v$ (m/sec)
v_r	Radial velocity component, with respect to local cylindrical coordinate system with origin at vortex core center (m/sec)
v_z	Axial velocity component, with respect to local cylindrical coordinate system with origin at vortex core center, flow along filament length (m/sec)
v_θ	Tangential velocity component, with respect to local cylindrical coordinate system with origin at vortex center (m/sec)
z	Axial coordinate, along axis of vortex filament, with respect to local cylindrical coordinate system with origin at vortex center (m)
$\delta(x)$	Dirac (“delta”) function; x is the argument
$\delta'(x)$	Derivative of Dirac (“delta”) function, $\delta'(x) = d(\delta(x))/dx$
γ	Vortex filament circulation initial value, at $t = 0$ (m^2/sec)
ν	Kinematic viscosity (m^2/sec)
Ω	Rotor rotational speed (radians/sec)
ρ	Freestream density (kg/m^3)
θ	Polar coordinate, with respect to local cylindrical coordinate system, referenced to the vortex core center and the shear layer/slipstream boundary (radians)
ψ	Stream function (m^2/sec)
ψ_*	Localized three-dimensional contribution to the vortex tangential velocity and vorticity, accounts for “line-sink” v_z flow at the shear layer boundary (m^2/sec)
$\tilde{\psi}$	“Mean” stream function scaler value, function of r only, where $\tilde{\psi} \equiv \int_0^{2\pi} (\psi + \psi_*) d\theta$, (m^2/sec)
ψ_w	Wake age (degrees)
$\Delta\psi_w$	Net required wake age for vortex filament decay/collapse (degrees)
ω	Flow vorticity

ROTOR VORTEX FILAMENTS: LIVING ON THE SLIPSTREAM'S EDGE

Larry A. Young

Ames Research Center

SUMMARY

The purpose of this paper is to gain a better understanding of rotor wake evolution in hover and axial flow by deriving an analytical solution for the time dependent behavior of vortex filament circulation and core size. This solution is applicable only for vortex filaments in the rotor far-wake.

A primarily inviscid vortex/shear layer interaction (where the slipstream boundary is modeled as a shear layer) has been identified in this analytical treatment. This vortex/shear layer interaction results in decreasing vortex filament circulation and core size with time. The inviscid vortex/shear layer interaction is shown, in a first-order treatment, to be of greater magnitude than viscous diffusion effects. The rate of contraction, and ultimate collapse, of the vortex filament core is found to be directly proportional to the rotor inflow velocity.

This new insight into vortex filament decay promises to help reconcile several disparate observations made in the literature and will, hopefully, promote new advances in theoretical modeling of rotor wakes.

INTRODUCTION

Even the most sophisticated of rotor free wake analyses neglect the decay of vortex filaments in their wake modeling. The assumption of constant vortex circulation and core size as adopted in free-wake analyses is too simplistic. And yet, to date, there is no new theoretical approach to replace this constant circulation and core size assumption. This dichotomy is noted in reference 1. Most insights into vortex filament decay have their roots in fixed-wing aerodynamics. But, as the author will contend in this paper, application of these fixed-wing observations to rotorcraft is unjustified and ultimately leads to erroneous conclusions.

What is not in dispute throughout the rotorcraft literature is that within three to five blade passages well-defined vortex filament structures can not be observed by means of any flow visualization technique. The analytical/computational treatment of the far-wake as evolving into an "ultimate" wake is, therefore, conceptually flawed. What has been the conventional wisdom, as regards this observed vortex filament decay in the far-wake, is that viscous diffusion effects are responsible for the process. Various turbulent vortex models, derived from fixed-wing analytical work, have been ad hoc modified and applied to attempt to account for, or match, the observed rotary-wing vortex

filament decay process. There has not been a fundamental re-examination of the vortex dynamics/fluid mechanics for rotor trailed vortices.

Other than qualitative flow visualization work, there is mixed empirical evidence for the time-dependent behavior of rotary-wing vortex filament circulation and core size. Most measurements have been made near, or before, the first blade passage. Correspondingly, these measurements have shown little wake age dependence of circulation and core size. Recent rotary-wing experimental observations, encompassing a greater range of wake ages than previously studied, are starting to appear in the literature. For example, one such study (A. Wadcock, Measurement of Vortex Strength and Core Diameter for a Model Tiltrotor, a soon to be published NASA CR) has presented hot-wire anemometry results that suggest that vortex circulation and core size both appear to decrease with wake age. This observation is counter to expectations based on the flow behavior of fixed-wing trailed vortices. However, an attempt to use the wide-field shadowgraph technique, reference 2, to measure rotor vortex core size as a function of wake age appeared to show the opposite trend from the Wadcock study. Reference 2 results implied that there was core size growth with wake age. Interestingly enough, both the Wadcock study and the reference 2 work conducted their vortex core size measurements with the same rotor/test-stand, in two different test entries. Both studies, though promising in their technique and initial results, should be considered as very preliminary bodies of work.

Another noteworthy set of studies for vortex circulation and core size trends with wake age is the laser velocimetry work of references 3–5. However, though the authors of these works have made impressive progress in their measurement techniques, they have, to date, relied upon rather simplistic rotor systems that are not representative of actual aircraft. In particular, they obtained their test results for one-bladed, low tip speed rotors. As will be discussed later in the paper, the geometry and operating condition of rotor test models will have a substantial impact on the observed vortex circulation and core size trends. More systematic work using realistic scaled rotor models is required before empirical observations provide definitive answers to the rotary-wing vortex decay process.

What is needed, more importantly though, is a fresh approach to the problem by reconsidering the fundamental differences between a trailed vortex filament from a fixed- and rotary-wing. The chief difference between the two types of trailed vortices, besides the helical geometry of the rotor vortex filament versus the rectilinear fixed-wing vortex, is that the rotor vortex is not surrounded by a uniform flow field as is the fixed-wing trailed vortex but is instead embedded in a shear layer. It is this flow feature, and the associated singular fluid mechanics, of a vortex in a shear layer that governs the decay process of a rotor trailed vortex filament. This area of investigation (vortex/shear layer interactions) has received very little analytical/computational work even though it would seem to be a fundamental type of fluid flow problem deserving considerable attention.

This paper addresses the above noted oversight by developing an analytical model of vortex filament decay that accounts for vortex/shear layer interactions and is applicable to hover and axial-flight rotor wakes.

This work is dedicated to the memory of Clara Jeannette McClelland Springer.

DESCRIPTION OF AN IDEALIZED FLOW PROBLEM AND ITS RELATIONSHIP TO ROTOR WAKES

Figure 1 shows a vortex filament in the far wake region of a rotor slipstream. Sufficiently downstream in the far-wake, the rotor slipstream flow is no longer accelerating and the boundary is no longer contracting. Further, the roll-up of vortex sheets inside the rotor wake has been completed and all vorticity is encompassed in the rotor trailed tip vortices. It is in the rotor far-wake that a number of simplifying assumptions can be made about the slipstream flow field, resulting in a “idealization” of the localized environment about a trailed vortex. First of all, the influence of wake contraction and nonuniform wake velocity profile will be neglected in this study. Further, the vortex filament helical angle and curvature can be assumed to be small and the flow problem can be treated as quasi-two-dimensional. Finally, the slipstream flow field is assumed uniform and the slipstream boundary is modeled as a discontinuous shear layer.

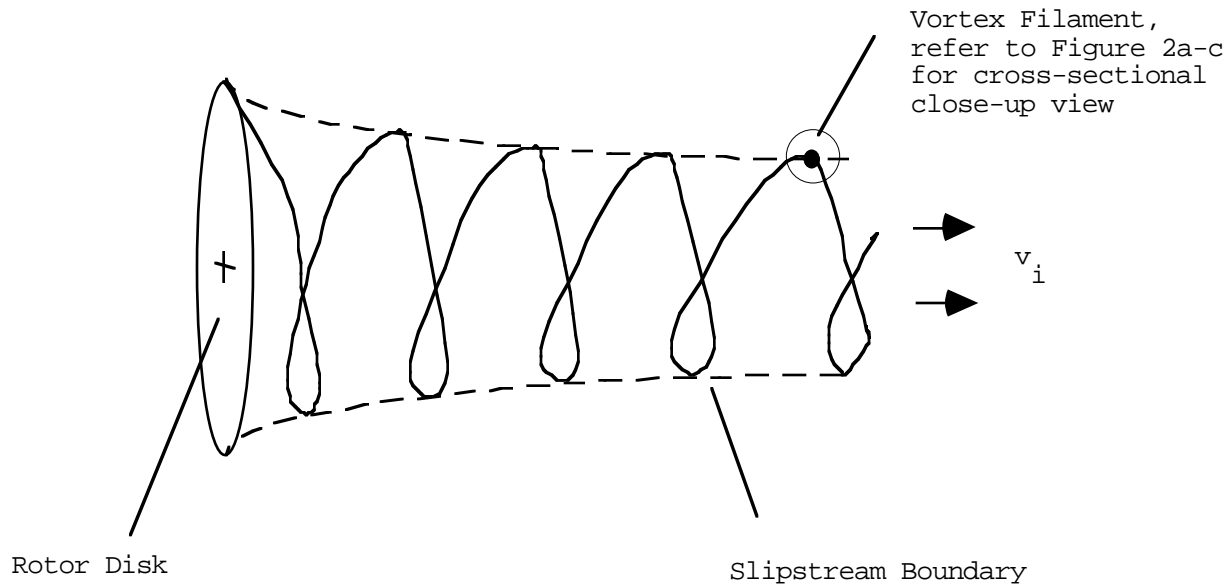


Figure 1. Vortex filament in the far-wake of a rotor slipstream.

Figures 2(a–c) illustrate the vortex filament fluid mechanics (in a two-dimensional plane) at the slipstream boundary. Helmholtz’s Law requires that a vortex filament generated at the rotor disk accelerates to an equilibrium velocity of $U + v_i/2$ along the slipstream boundary. The local cylindrical coordinate system chosen for the idealized flow problem tracks along with an isolated vortex core center at this velocity of $U + v_i/2$. Consequently, the velocity inside the shear layer is $+v_i/2$, while outside it the velocity is $-v_i/2$. This shear layer in the idealized flow problem is prescribed, time-invariant, and discontinuous.

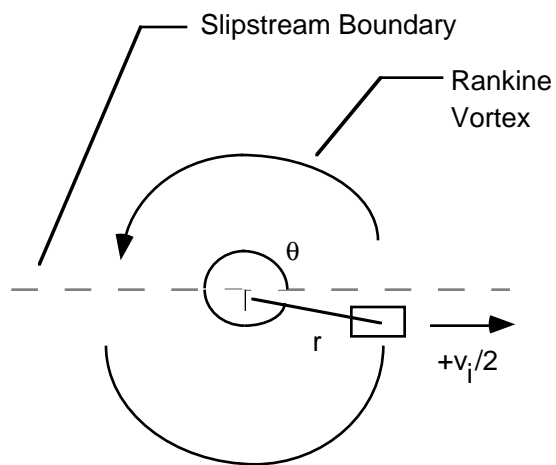


Figure 2a - Radial velocity of unit volume of fluid just prior to crossing slipstream boundary, while within rotor wake.

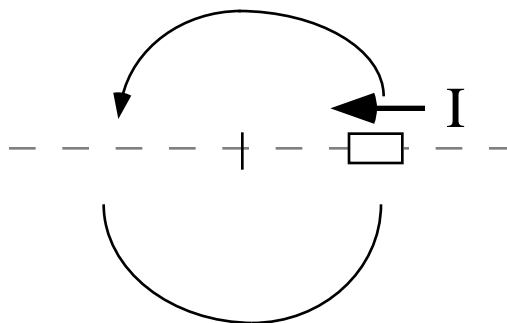


Figure 2b - Unit volume of fluid subjected to impulsive force when crossing slipstream boundary.

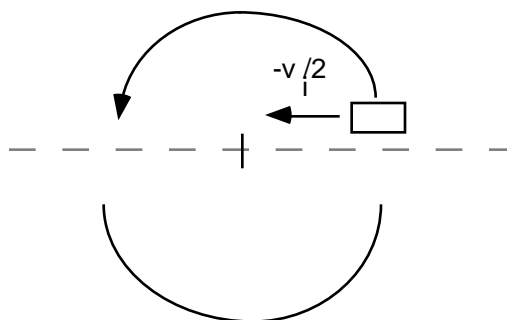


Figure 2c - Radial velocity of unit volume of fluid just after crossing slipstream boundary; impulsive force results in momentum change.

Figure 2. Problem description.

Figures 2(a–c) illustrate a “thought experiment” that asserts the existence of impulsive forces at the rotor slipstream boundary. Figure 2(a) depicts a unit volume of fluid prior to crossing the slipstream boundary, while it is still within the rotor wake proper; the unit volume has a radial velocity of $+v_i/2$. Figure 2(b) shows that the unit of volume of fluid, as it crosses the slipstream boundary, is subjected to an impulsive force. Figure 2(c) depicts the unit volume of fluid after crossing the slipstream boundary and just entering the freestream; the unit volume now has a radial velocity of $-v_i/2$. Consequently, the impulsive force applied to the unit volume of fluid as it crosses the slipstream has resulted in a net momentum change. This process occurs at $\theta = 0$, which is shown in figures 2(a–c), and is repeated at $\theta = \pi$ (which is not shown). Force equilibrium is thus preserved as the impulsive force generated at $\theta = 0$ acts in opposition to the force at $\theta = \pi$.

The vortex/slipstream shear layer interaction is assumed to be primarily an incompressible, inviscid flow phenomenon. It would seem, upon first consideration, that assuming inviscid flow while studying vortex filament decay does not make sense. Yet, it will ultimately be shown that the inviscid shear layer influence on vortex core size is much larger than viscous diffusion effects.

Discontinuous shear layers, whether viscous or inviscid, are unstable (refs. 6 and 7). A rotor slipstream, or any naturally occurring shear layer, will consequently have a finite but steep shear flow gradient across its boundary. Nonetheless, a prescribed, time-invariant, discontinuous shear layer is very convenient as an idealization of a rotor slipstream. Because the shear layer is prescribed, and not part of the flow solution proper, the overall flow will not be subject to the instabilities noted in reference 7.

It is the existence of these hypothesized impulsive forces, which are generated as vortical flow crosses the shear layer boundary, that makes rotor vortex filament decay uniquely and radically different from fixed-wing trailed vortex decay. The above thought experiment and corresponding idealization of the flow problem invoke fairly extreme simplifying flow assumptions. And, yet, the analytical solution of the described flow problem can and should be thought of as a “limiting case” for more physically realistic descriptions of the vortex/shear layer interaction.

A Rankine vortex will be used to model the rotor tip vortex filaments in this paper. The analysis will assume that the Rankine vortex is isolated from the influence of other vortices along the slipstream boundary. A Rankine vortex was chosen for this analysis because of the simplicity of its modeling.

SUMMARY OF THE APPLICABLE GOVERNING EQUATIONS FOR THE DESCRIBED PROBLEM

Equations 1–4 are the governing equations for the vortex/shear interaction. Equation 1a is the incompressible r-momentum (cylindrical coordinate) Navier-Stokes equation. Equation 1b is a derivative form of the r-momentum equation that has been integrated with respect to θ . Refer to appendix A for further details of the transforming equation 1a to 1b. Equation 1c explicitly includes the impulsive forces at $\theta = 0$ and $\theta = \pi$ in the r-momentum equation.

$$\frac{\partial v_r}{\partial t} + v_r \frac{\partial v_r}{\partial r} + \frac{v_\theta}{r} \frac{\partial v_r}{\partial \theta} + v_z \frac{\partial v_r}{\partial z} - \frac{v_\theta^2}{r} = F + v \left(\nabla^2 v_r - \frac{v_r}{r^2} - \frac{2}{r^2} \frac{\partial v_\theta}{\partial \theta} \right)$$

↓

(1a-b)

$$\frac{\partial}{\partial t} \left(\int_0^{2\pi} v_r d\theta \right) + \int_0^{2\pi} \left\{ v_r \frac{\partial v_r}{\partial r} + \frac{v_\theta}{r} \frac{\partial v_r}{\partial \theta} \right\} d\theta \approx -2v_i \frac{\partial v_\theta}{\partial r} \Big|_{\theta=0,\pi}$$

where F in equation 1a is given by

$$F = -\frac{1}{\rho} \frac{\partial P}{\partial r} + g_r + \frac{1}{\rho} \frac{\partial}{\partial r} \{ I [\delta(\theta) + \delta(\theta - \pi)] \} \quad (1c)$$

The key modeling assumptions employed in equation 1b are: the flow is inviscid; the flow is quasi-two-dimensional such that $\partial v_r / \partial z = \partial v_\theta / \partial z = \partial v_z / \partial z = 0$, except that $\partial v_z / \partial z = (1/v_z)(\partial v_z / \partial t) \neq 0$ when $\theta = n\pi$, for $n = 0, 1, 2, \dots$; the radial pressure gradient is primarily due to the vortex tangential flow $\rho v_\theta^2 / r \approx \partial P / \partial r$ for $\theta \neq n\pi$; the impulsive force can be related to the net momentum change across the discontinuous shear layer by

$$\frac{1}{\rho} \frac{\partial}{\partial r} \left\{ \int I [\delta(\theta) + \delta(\theta - \pi)] d\theta \right\} = -2v_i \frac{\partial v_\theta}{\partial r} \Big|_{\theta=0,\pi}$$

Equation 2a is an identity that follows straightforwardly from differential calculus. Definition of the two new parameters, $\tilde{\psi}$ and ψ_* , eliminates θ from the identity. Refer to appendix B for additional details as to the definition and application of equations 2a-b.

$$\frac{\partial r}{\partial t} \Big|_{r=r_c} = \frac{1}{\left(\frac{\partial \tilde{\psi}}{\partial r} \right)} \cdot \frac{\partial \tilde{\psi}}{\partial t} \Big|_{r=r_c} \quad (2a)$$

where

$$\tilde{\psi} \equiv \int_0^{2\pi} (\psi + \psi_*) d\theta \quad (2b)$$

Note that in equation 2b and in subsequent use in this paper, ψ_* is the localized three-dimensional contribution to the vortex tangential velocity and vorticity, that accounts for nonzero v_z flow at the shear layer boundary.

Equation 3a is the general form of the vorticity conservation equation. Equation 3b is the derivative form of the conservation equation for a control volume about the vortex core boundary. This

integro-differential equation models the entrainment of negative vorticity into the vortex core; this negative vorticity is generated by the vortex/shear layer interactions. Refer to appendix B for details of transforming equation 3a to 3b.

$$\begin{aligned} \frac{\partial}{\partial t} \left(\int \omega dV \right) + \int (\omega \cdot n) u dS &= \int (n \times F) dS \\ \downarrow \\ \frac{\partial}{\partial t} \left\{ \int_0^{2\pi} \int_0^{r_c g(t)} \nabla^2 (\psi + \psi_*) r dr d\theta \right\} &= \int_0^{2\pi} \left\{ \frac{\partial \psi}{\partial \theta} + r_c^2 \frac{d}{dt} g(t) \right\} \nabla^2 (\psi + \psi_*) d\theta \Big|_{r=r_c} \end{aligned} \quad (3a-b)$$

The ψ_* contributions to the vorticity conservation equation can be clearly seen in equations 3a–b. Note that $\nabla^2(\psi + \psi_*)$, and not $\nabla^2\psi$, are used to define the vorticity. But, alternatively, $\partial\psi/\partial\theta$ is used to define the vorticity convection velocity into the vortex control volume.

Equation 4a is the incompressible z-momentum (cylindrical coordinate) Navier-Stokes equation. Equation 4b is a derivative form of the z-momentum equation. Refer to appendix C for the assumptions and approximations employed in reducing equation 4a to 4b.

$$\begin{aligned} \frac{\partial v_z}{\partial t} + v_r \frac{\partial v_z}{\partial r} + \frac{1}{r} v_\theta \frac{\partial v_z}{\partial \theta} + v_z \frac{\partial v_z}{\partial z} &= -\frac{1}{\rho} \frac{\partial P}{\partial z} + \nu \nabla^2 v_z \\ \downarrow \\ \frac{\partial v_z}{\partial t} + \frac{1}{r} v_\theta \frac{\partial v_z}{\partial \theta} + v_r \frac{\partial v_z}{\partial r} &= 0 \end{aligned} \quad (4a-b)$$

Equations 1–4 are not dependent upon the type of finite-core vortex model employed in the analysis. The governing equations could be applied to any vortex model such as the Rankine or the Scully model (ref. 8).

SUMMARY AND DISCUSSION OF A SOLUTION FOR A RANKINE VORTEX AS APPLIED TO THE DESCRIBED PROBLEM

An analytical solution describing the decay of a Rankine vortex embedded in the shear layer of a steady, uniform slipstream is detailed in appendices A–C and summarized in equations 5–11 in the main body of this paper.

The vortex/shear layer stream function ($\psi + \psi_*$) that satisfies equations 1a–c has a spiral-like distribution in the region $r_c < r < r_o$ (fig. 3). This spiral-like behavior of rotor vortex filaments is empirically well documented in the literature (e.g., refs. 9 and 10). Flow inside the rotor slipstream

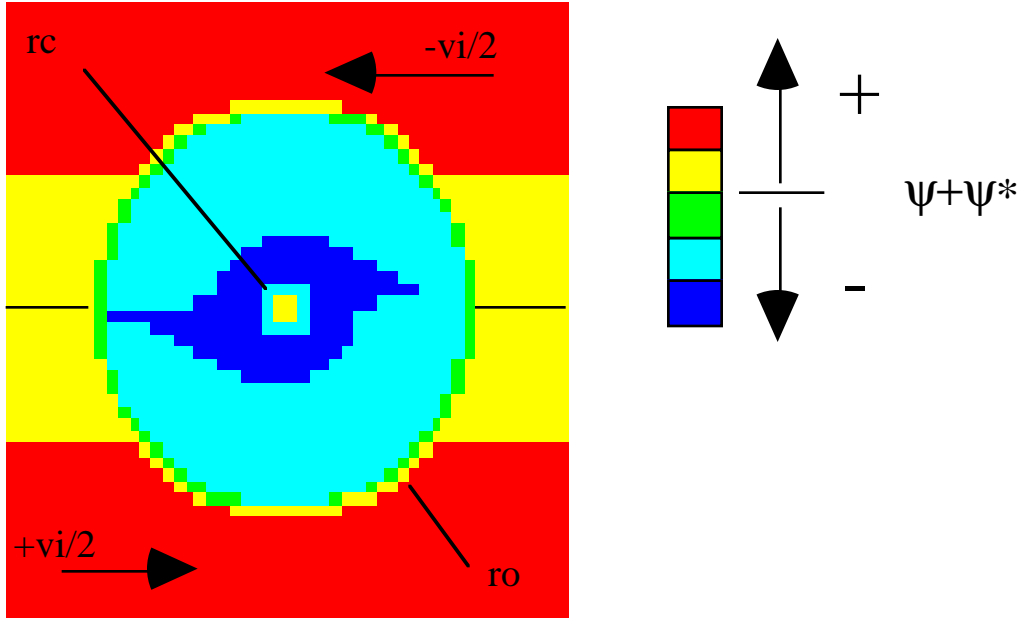


Figure 3. Stream function ($\psi + \psi_*$) (eqs. 5a–b).

is shown in the lower half-plane of figure 3, and the flow outside the slipstream is in the upper half-plane. Equations 5a–b describe the vortex/shear layer stream function.

$$\psi = -\frac{1}{2} v_i \text{sgn}(\theta - \pi) r \sin \theta + \frac{\gamma}{4\pi} f(t) \left\{ \ln(r) [1 + \text{sgn}(r - r_c)] + \frac{1}{2} \left(\frac{r}{r_c g(t)} \right)^2 [1 + \text{sgn}(r_c - r)] \right\} + kr\theta \quad (5a)$$

where

$$k = \frac{v_i}{4} \quad (5b)$$

and

$$\psi_* = -\pi kr \text{Int} \left(\frac{\theta + \pi}{\pi} \right) \quad (5c)$$

Sgn(x) and Int(x) are the “signum” and “integer” functions, respectively. The constant k is proportional to the rate that the vortex core decays; the constant v_i is the far-wake velocity, which is found from simple rotor momentum theory. Refer to appendix A for the details of the stream function derivation.

The stream function, equations 5a–c, is valid for a finite radial region defined by

$$r_c g(t) \leq r < \frac{\gamma}{2\pi^2 k} f(t)$$

The “finiteness” of the applicable flow region of the stream function is very important. It circumvents the prediction of physically unrealistic flow behavior far from the vortex core by confirming that the vortex/shear layer interaction is a “localized” phenomenon.

The stream function, as written in equations 5a–c, is also subject to the flow constraint

$$(\partial \psi_{\text{Slipstream Flow}} / \partial r) / (\partial \psi_{\text{Vortex}} / \partial r) > 0$$

This flow constraint confirms that the stream function has been written to conform to the flow representative of rotary-wing slipstreams and vortices. Alternatively, bluff body wakes and shed vortices do not conform to this flow constraint. This issue will be discussed further later in the paper.

A consequence of the derived stream function, equations 5a–b, is that negative vorticity is generated by the vortex/shear interaction (see eq. 6).

$$\omega = -\frac{1}{r} k \left\{ \theta - \pi \text{Int} \left(\frac{\theta + \pi}{\pi} \right) \right\} + \frac{\pi k}{r} \delta'(\theta - \pi) + \frac{v_i}{r} \{ 2\delta(\theta - \pi) \cos \theta + \delta'(\theta - \pi) \sin \theta \}$$

for $r \geq r_c g(t)$ (6)

Equation 6 demonstrates that just as impulsive forces exist for a vortex embedded in a discontinuous shear layer, so does impulsive changes in vorticity. Most importantly, negative vorticity is created at the shear layer and will be shown to be convected/entrained into the vortex core. This result, equation 6, is crucial for the discussion that follows for the time-dependent behavior of the vortex filament circulation and core size—i.e., the decay process itself. Refer to appendix B for details to the vorticity expression, equation 6, derivation.

The velocity and stream-function relationships used in this paper are subtly different from their conventional definition. They have been modified to account for quasi-two-dimensional flow. Quasi-two-dimensional flow has been defined in this paper as allowing localized, nonzero, time-dependent axial flow ($v_z \neq 0$ at $\theta = 0$ and $\theta = \pi$, whereas $v_z = 0$ for $\theta \neq n\pi$ where $n = 0, 1, 2, \dots$) along the shear layer boundary. The velocity and stream function definitions have been modified such that now $v_\theta \equiv +\partial(\psi + \psi_*)/\partial r$ and $v_r \equiv -(1/r)(\partial\psi/\partial\theta)$. The tangential velocity expression has picked up an additional stream function term, ψ_* , as compared to its conventional definition.

The consequence of this quasi-two-dimensional flow revision to the stream function and velocity definition, when applied to the vortex/shear layer interaction problem, is that a constant radial flow into the vortex center is predicted, as well as an asymmetric tangential velocity distribution (see eqs. 7–8). The tangential velocity asymmetry can be seen in figure 4. The velocity profile shown in figure 4 is along the slipstream boundary ($\theta = 0$ and $\theta = \pi$). Therefore, the asymmetry shown in

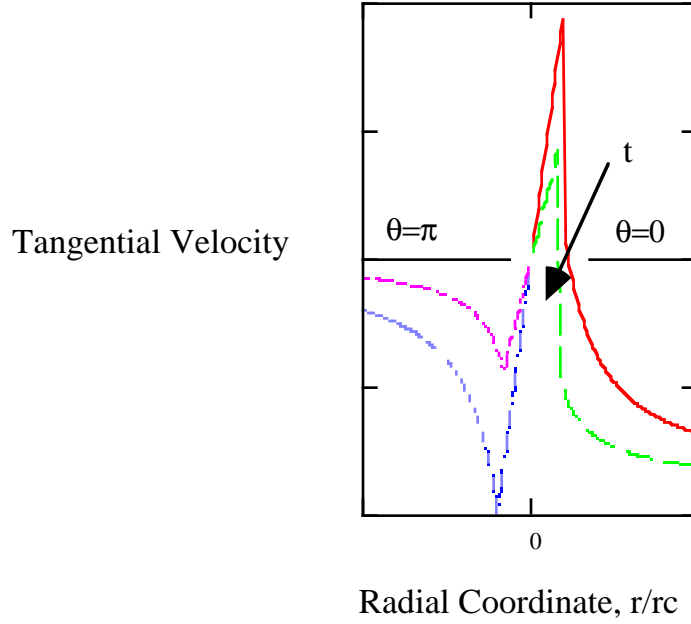


Figure 4. Decay of vortices on a rotor slipstream boundary.

figure 4 is distinct from the asymmetry encountered/expected when crossing the slipstream boundary (i.e., $\theta = \pi/2$ or $3\pi/2$).

$$v_{\theta} = -\frac{1}{2} v_i \operatorname{sgn}(\theta - \pi) \sin \theta + \frac{\gamma}{4\pi} f(t) \left\{ \left(\frac{1}{r} \right) [1 + \operatorname{sgn}(r - r_c)] + \frac{r}{r_c^2 g(t)^2} [1 + \operatorname{sgn}(r_c - r)] \right\} + k \left(\theta - \pi \operatorname{Int} \left(\frac{\theta + \pi}{\pi} \right) \right) \quad (7)$$

$$v_r = \frac{1}{2} v_i \operatorname{sgn}(\theta - \pi) \cos \theta - k \quad (8)$$

Derivation of radial and tangential velocity analytical expressions follow directly from the derived stream function, equations 5a–b.

Radial flow and vorticity entrainment into the vortex core causes the vortex circulation to be time dependent. Vortex circulation is found to be a decreasing function of time and wake age. Refer to equations 9a–b and figure 5.

$$\text{Circulation} = \gamma f(t) \quad (9a)$$

where

$$f(t) = \left(\frac{2\pi^2 r_c k}{3\gamma} \right) g(t) + \left(1 - \frac{2\pi^2 r_c k}{3\gamma} \right) g(t)^4 \quad (9b)$$

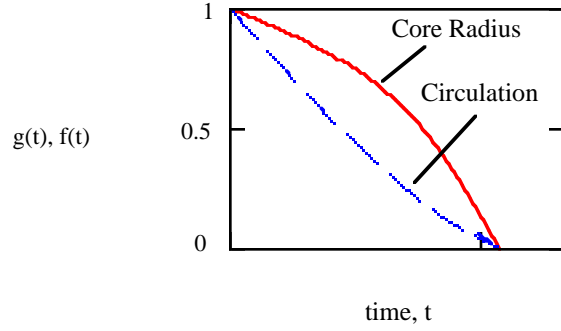


Figure 5. Vortex circulation and core size as a function of time (eqs. 9 and 10).

γ and r_c are the initial values, respectively, of vortex circulation and vortex core radius. The function $g(t)$ is defined in equation 10b. The function $f(t)$ encompasses the time dependency of vortex circulation. The function $g(t)$ reflects the time dependency of the vortex core size. Refer to appendix B for the details of the derivation of the above analytical expression for the vortex circulation decay. The rate of decay of circulation can be seen to be directly proportional to rotor inflow velocity. Identification of a potential flow mechanism that results in decreasing circulation is quite surprising.

Even more surprising is the analytical result for the time dependence of the vortex core size. Core size is also found to decrease with time and wake age. Refer to equations 10a–b and figure 5.

$$\text{Core Radius} = r_c g(t) \quad (10a)$$

where

$$\gamma f(t) + \pi^2 k r_c g(t) = \pi^2 k r_c + \gamma - (2v_i k + \pi^2 k^2) t \quad (10b)$$

r_c is the initial value for the vortex core radius; equation 5b provides the value of the constant, k .

Equations 9b and 10b are a nonlinear, simultaneous set of equations that are iteratively solved for $f(t)$ and $g(t)$ for each time, t . Refer to appendix B for the details of the derivation of the solution of the vortex circulation and core size time dependent behavior.

The prediction of vortex core size contraction is contrary to conventional thinking, which is based in large part upon observations made from rotary-wing flow visualization studies. This discrepancy will be discussed further later in this paper. But a key consideration in interpretation of rotor wake flow visualization results is the assumption of the relative magnitude of axial flow, v_z , along the vortex filament length.

Work from this paper (eqs. 11a–b) predicts large vortex filament axial velocities along the shear layer boundary.

$$v_z = e^{\pi k \delta(\theta - n\pi)t/r} \quad \text{for} \quad t \ll \Delta\psi_w/\Omega \quad (11a)$$

$$v_z \rightarrow Ae^{\text{sgn}(\theta - \pi)r \sin \theta} \quad \text{for} \quad t \rightarrow \infty \quad (11b)$$

where

$$A \approx -2 \frac{v^2}{V_T} \sqrt{\ln(V_T^2 + v^2) - 2 \ln(v)} \quad (11c)$$

Refer to appendix C for details of the axial flow solutions. Equation 11a describes a “line-sink.” A portion of the mass flow crossing the slipstream boundary is redirected and convected axially along the shear layer. Equation 11a is a limiting case for more realistic shear layer models (where shear layer gradients are steep but not discontinuous), and so equation 11a suggests that axial velocities for rotor tip vortices are large, but finite, and increase with time. Ultimately, at $t \rightarrow \infty$, the axial velocity distribution of the asymptotic solution, equation 11b, suggests that a swirl distribution develops at the slipstream boundary that counterbalances the swirl in the rotor slipstream from the blade root vortex. Through equivalence of kinetic energy (an energy balance between the swirl from the blade-root vortex versus that of the swirl induced from the trailed tip vortices), the constant A was defined, equation 11c.

RE-EXAMINATION OF THE ANALYSIS ASSUMPTIONS IN LIGHT OF THE DERIVED SOLUTION

It might be supposed that reliance on an inviscid analysis could result in invalid conclusions as to vortex filament circulation and core size time-dependent behavior. A first-order examination of the relative contraction and expansion rates of inviscid versus viscous effects will show that the inviscid vortex/shear layer interaction dominates the fluid dynamics of rotor vortex filaments. Examining more closely this assertion, i.e.,

$$\left| \frac{\partial r_c}{\partial t} \right|_{\text{Inviscid Vortex/Shear Layer Interaction}} \gg \left| \frac{\partial r_c}{\partial t} \right|_{\text{Viscous Trailed Vortex Decay}} \quad (12a)$$

For $t \gg 0$, the predicted inviscid vortex core contraction rate will be compared to the viscous diffusion rate of a Lamb-Oseen laminar trailed vortex (ref. 11). Or

$$\left. \frac{\partial r_c}{\partial t} \right|_{\text{Inviscid Vortex/Shear Layer Interaction}} \rightarrow -\left(\frac{2}{\pi^2} + \frac{1}{4} \right) v_i \quad (12b)$$

$$\left. \frac{\partial r_c}{\partial t} \right|_{\text{Viscous Trailed Vortex Decay}} = 1.12 \sqrt{\frac{v}{t}} \quad (12c)$$

Using typical values for v_i and v for equations 12a–c, the inviscid contraction rate is estimated as being a couple of orders of magnitude greater than the laminar vortex core expansion rate. For example, for $\Delta\psi_w > 2$ degrees ($t \gg 0$), the laminar expansion rate is less than 0.1 foot per second. But, for a hovering rotor, for $0.01 < C_T < 0.015$, which is typical of 1G thrust loaded rotors, the predicted inviscid contraction rate is 50 to 60 feet per second. Some authors have suggested that the contribution of turbulent viscosity to a trailed vortex diffusion rate may be as much as an order of magnitude greater than the laminar estimate (see ref. 3). Nonetheless, if this supposition was proven correct for rotor trailed vortices, the inviscid vortex/shear layer interaction contraction rate is still greater than this inflated viscous diffusion rate estimate. Therefore, the inviscid flow assumption employed in the beginning of this paper appears to be, ultimately, justifiable.

Another assumption employed in this paper's analysis that bears further scrutiny is that the radial pressure gradient is dominated by quasi-steady vortical flow. That is, it has been assumed that

$$\frac{v_\theta^2}{r} \approx \frac{1}{\rho} \frac{\partial P}{\partial r} \quad (13)$$

The static pressure can be separated into two components: a quasi-steady pressure component that is dominated by the vortex flow and an unsteady, non-vortex-driven pressure component from the vortex/shear layer interaction. That is: $P = P_{QSV} + P_{UNV}$. The implication of this observation is that the above assumption (eq. 13) is equivalent to the assertion represented by equations 14a–c (for $\theta \neq 0 \neq \pi$ where the pressure gradient contribution to the surface forces has been encapsulated in the impulsive shear forces, $I(\delta(\theta) + \delta(\theta - \pi))$, which have been explicitly separated out):

$$\left| \frac{\partial P_{QSV}}{\partial r} \right| \gg \left| \frac{\partial P_{UNV}}{\partial r} \right| \quad (14a)$$

where the respective terms are

$$\frac{\partial P_{QSV}}{\partial r} \equiv \rho \frac{v_\theta^2}{r} = \frac{\rho}{r} \left(\frac{\partial \psi}{\partial r} \right)^2 \quad (14b)$$

$$\frac{\partial P_{UNV}}{\partial r} \equiv -\rho \left\{ \frac{\partial v_r}{\partial t} + v_r \frac{\partial v_r}{\partial r} + \frac{v_\theta}{r} \frac{\partial v_r}{\partial \theta} \right\} \rightarrow -\rho \frac{v_\theta}{r} \frac{\partial v_r}{\partial \theta} = \frac{\rho}{r^2} \left(\frac{\partial \psi}{\partial r} \right) \left(\frac{\partial^2 \psi}{\partial \theta^2} \right) \quad (14c)$$

Therefore, if equation 13 is true then, given equations 14a–c, the inequality constraint can be re-written as

$$\left| \frac{\partial \psi}{\partial r} \right| \gg \frac{1}{r} \left| \frac{\partial^2 \psi}{\partial \theta^2} \right| \quad (15a)$$

Or, making substitutions from equation 5a–b,

$$\frac{\gamma}{2\pi} \frac{f(t)}{r} + k \left\{ \theta - \pi \text{Int} \left(\frac{\theta + \pi}{\pi} \right) \right\} \gg 0 \quad (15b)$$

Using typical values for $f(t)$, k , r_c , and γ , the left hand side of the equation 15b inequality is found to be quite large—one to two orders of magnitude greater than unity. Using the reference 2 values for $f(t)$, k , r_c , and γ , the ratio r/r_c has to be greater than the value of 4.2 before the magnitude of the left hand side of the inequality drops below unity. The stream function is valid to only $r_o/r_c = 4.3$. The flow assumption represented by equation 13 thus appears valid.

Besides viscous flow effects, the distributed vorticity of real rotor vortices versus the concentrated vorticity in the core of a Rankine vortex and the interactional influence of multiple rotor tip vortices on each other will each tend to counterbalance the predicted core collapse. Additionally, the influence of rotor slipstream acceleration on the vortex circulation and core size time dependent behavior needs to be assessed in further work.

IMPLICATIONS OF THE VORTEX/SHEAR LAYER INTERACTION SOLUTION WITH RESPECT TO OBSERVATIONS MADE IN THE LITERATURE

The predicted flow characteristics from this paper's work provide insight into several puzzling and conflicting observations made in the literature regarding rotor wake behavior. Using the analytical results from this paper, many of these observations can at least be partially reconciled with each other.

As noted earlier, a key empirical observation for rotor wakes, as reported innumerable times in the literature, is that the rotor far wake loses, after three to five blade passages, its well-defined vortex

filament structure. Previously, the decay mechanism for the far-wake trailed vortex filaments has been assumed to be due to viscous diffusion of the filament vorticity. This paper has promoted an alternate hypothesis and interpretation of the filament decay mechanism and, further, has derived a solution for this inviscid vortex/shear layer interaction that predicts vortex circulation and core size to decrease with time/wake age.

But, as noted earlier, the prediction of vortex core size contraction is contrary to conventional thinking. Most experimental studies reported in the literature on rotor wakes and vortex core size measurements have relied on smoke or particle flow visualization or, alternatively, velocity measurements near the rotor disk plane. The vortex core has been equated, or assumed directly proportional, to observed “particle voids” in vortex filaments for seeded rotor wakes. And, indeed, these vortex filament particle voids, for rotor wakes, do grow in size with time/wake age. However, the author asserts that smoke flow visualization is an invalid measure of vortex core size.

The fascinating flow visualization photographs of reference 12 are the clearest illustration that the smoke particle void is not the same as the vortex core. In the reference 12 photographs, smoke flow visualization results (i.e., the particle void) are observed simultaneously with fortuitous images of the vortex core as seen by means of condensation. In many cases, the smoke particle void is much greater in size than the vortex core.

Smoke flow visualization results are an invalid measure of vortex core size because of the influence of large axial velocities, v_z , existing along the vortex filament length that sweep regions greater than the vortex core clear of smoke particles. There is considerable analytical and experimental work that confirms the existence of large axial velocities along a trailed vortex filament length. The prediction of nonzero axial velocity along the vortex filament length, as derived in this paper, qualitatively agrees with helium bubble flow visualization observations recounted in references 1 and 13. Finally, the rotor swirl at the slipstream boundary that is implicit in the asymptotic axial velocity solution, equation 11b, matches qualitatively rotor wake swirl measurements noted in reference 10. Refer to figure 6.

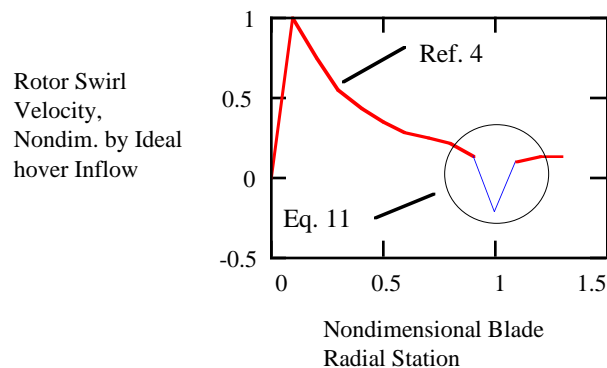


Figure 6. Swirl distribution of the rotor far wake, accounting for the asymptotic filament axial flow resulting from the inviscid vortex/shear layer interaction.

On the basis of both measurements and predictions, axial velocities are clearly of a magnitude to invalidate the assumption that the particle void at the center of a vortex is representative of the vortex core radius. The particle void as seen in smoke visualization work should asymptotically approach the value of $r_o(0)$ —where $r_o(t) = \gamma f(t)/2\pi^2 k$ and so $r_o(0) = \gamma/2\pi^2 k$ —rather than $r_{cg}(t)$. This hypothesis can be tested in future studies by comparing predicted $r_o(0)$ values to particle void trends. (Reference 13 is one of few studies in the literature to provide quantitative data of the particle void size trends with wake age. Unfortunately, reference 13 did not examine large enough wake ages for an asymptotic limit to be observed.) If the above hypothesis is true, i.e., the particle void is proportional to the $r_o(0)$, the asymptotic wake age limit for particle void size will be dependent upon tip speed and blade count for hovering rotors.

The apparent discrepancies in vortex core size trends between the work of A. Wadcock (Measurement of Vortex Strength and Core Diameter for a Model Tiltrotor, a soon to be published NASA CR) and the shadowgraph results of reference 2 can be commented on in light of the predictions of this paper. The study by Wadcock made hot-wire anemometry measurements of v_θ and was, therefore, able to directly estimate core size. The shadowgraph results of the reference 2, on the other hand, would tend to be biased towards a measure of the resultant velocity vector, i.e., $\sqrt{v_z^2 + v_\theta^2 + v_r^2}$, and not just v_θ . Interestingly enough, smoke flow visualization and shadowgraph test results will both be adversely impacted as a measure of vortex core size by not being able to account for non-negligible axial velocities, v_z , along the filament lengths.

The majority of research into rotor vortex circulation and core size trends with wake age have relied upon small-scale, low thrust, and low tip speed rotors. Also, one-bladed rotors have often been tested to keep the wake geometry as simple as possible. See references 3 and 13, for example. There is a critical scaling issue, though, in the use of small-scale, low tip-speed rotors and one-bladed rotors for studying vortex decay mechanisms and generalizing the results to rotors more representative of flight hardware (refer to eq. 16).

$$\Delta\psi_w = \left(\frac{\pi^2 + 8}{4} \right) \left(\frac{\Omega r_c}{v} \right) + \left(\frac{2\pi^2 + 16}{\pi N} \right) \left(1 + \frac{U}{v} \right) \quad (16)$$

where $\Delta\psi_w$ is the net amount of wake age required for decay of rotary-wing vortex filaments. Refer to appendix B for details of the derivation of equation 16. The derivation of this wake age expression for vortex decay follows directly from the nonlinear expressions for the vortex core size and circulation, equations 9a–b and 10a–b.

Examining equation 16 closely, the equation suggests that one-bladed rotor test results can potentially provide misleading insights into vortex circulation and core size trends. The vortex filament decay of the rotor studied by A. Wadcock (Measurement of Vortex Strength and Core Diameter for a Model Tiltrotor, a soon to be published NASA CR)—a small-scale rotor but with typical blade count and tip speeds for full-scale rotorcraft—is predicted to occur over roughly $\Delta\psi_w = 60$ –80 degrees. The reference 3 rotor (low tip speed and a single rotor blade) theoretically takes five times longer to decay out, i.e., $\Delta\psi_w = 300$ –400 degrees. Reference 3 identified a gradual decrease in circulation with wake ages in the far wake region; mixed results were seen for the core

size trend—though the authors ultimately concluded that there was overall growth in core size with time. Because of the intrinsically lower vortex decay rate for the reference 3 rotor, these results can not be considered conclusive.

Figures 7 and 8 provide a more detailed examination of the relative influence of blade count, thrust loading, and axial-flight (or climb) advance ratio on the predicted decay rate, which is inversely proportional to $\Delta\psi_w$, for the vortex core collapse. Both figures are based on predictions from equation 16. Figure 7 shows the influence of thrust and axial-flight advance ratio on $\Delta\psi_w$. Both rotor thrust and axial-flight advance ratio have a profound effect on the decay rate of trailed vortex filaments. Increasing axial-flight (or climb) advance ratio decreases the decay rate. An interesting interpretation of figure 7 is that as the axial-flight advance ratio asymptotically approaches infinity the rotary-wing vortex filaments will appear and behave almost like fixed-wing trailed vortices. At high axial-flight advance ratios the inviscid vortex/shear layer interaction becomes negligible and viscous diffusion will dominate the vortex decay process just as it does for fixed-wing trailed vortices. Figure 8 shows the influence of blade count and thrust for hovering rotors on $\Delta\psi_w$. In hover, rotor thrust has little impact on vortex decay rate, but increasing blade count and tip speed substantial increases the decay rate.

An interesting question is what happens to the vortex core size and circulation trends if the vortex tangential flow is counter to the slipstream flow, i.e., $(\partial\psi_{\text{Slipstream Flow}}/\partial r)/(\partial\psi_{\text{Vortex}}/\partial r) < 0$. This type of vortex/shear layer interaction is now representative not of the flow field of a rotor wake but is instead applicable to bluff body/shed vortex flow. It is asserted that equations 5–11 will also hold for bluff body/shed vortex flow—if the analysis is implemented with a change in sign of vortex circulation and the constant k (but not the value of the constant).

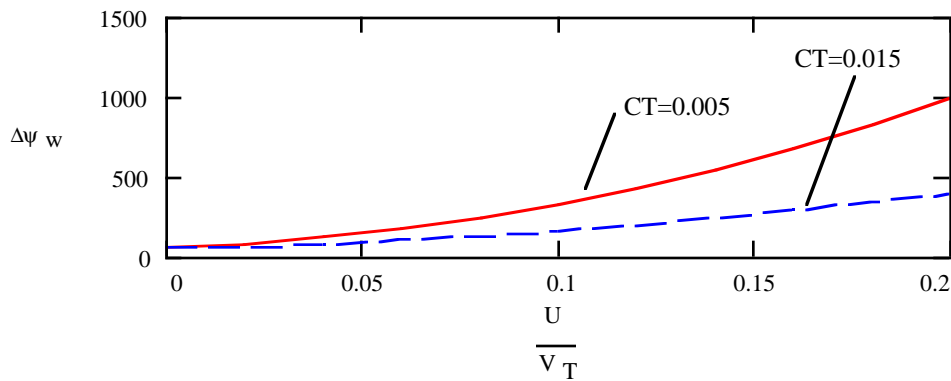


Figure 7. Vortex decay rate as a function of thrust and axial flow advance ratio (three bladed rotor).

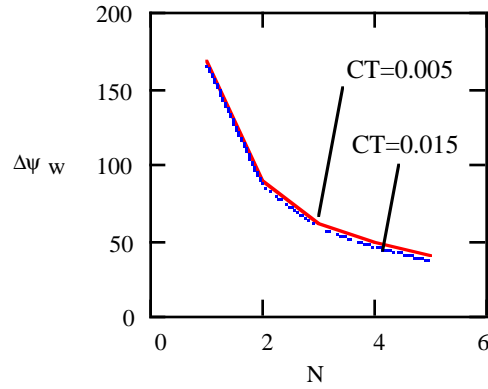


Figure 8. Vortex decay rate as a function of thrust and blade count for a hovering rotor.

To test this assertion, the results of this revised implementation of equations 5–11 will be qualitatively compared to the results of a computational fluid dynamics (CFD) treatment of the bluff body vortex/shear layer problem. Reference 14 is one of the few analytical or computational treatments of the vortex/shear layer problem. In the particular case of reference 14, a vortex embedded in a viscous, constant shear flow gradient was studied with an unsteady, Navier-Stokes CFD code. Given the reference 14 definition of the vortex/shear layer Reynolds number, the discontinuous, inviscid shear layer studied in this paper would yield $Re \rightarrow \infty$. A qualitative comparison can be made between this paper's analysis and the reference 14 results by studying the reference 14 high Reynolds number cases ($Re > 1000$). In both cases, vortex circulation increases rapidly in strength with time. No predictions were made in reference 14 for core size trends; equations 5–11, however, predict a slow growth of core size with time.

Despite this initial attempt to reconcile the experimental work of the past with the results of this paper, additional experimental investigations are necessary to corroborate and extend the analytical work described in this paper. Work in this area, concentrating on nonintrusive flow measurements that survey a large range of wake ages, is critical to understanding vortex filament decay mechanisms for rotors. Acquiring test data for more realistic rotor models is also crucial.

CONCLUSION

Many rotary-wing analyses rely upon the assumption of constant vortex circulation and core size in their formulation. However, an analytical treatment of vortex/shear layer interaction suggests that there is a substantial time (or wake age) dependence of vortex circulation and core size. Both are shown to decrease with time. The results of this paper will, hopefully, promote new insights into rotor wake flow behavior.

APPENDIX A – STREAM FUNCTION

Derivation of the Governing Equation

Beginning with the three-dimensional, incompressible r-momentum Navier-Stokes equation for a vortex embedded in a shear layer (cylindrical coordinates, with the origin centered on the vortex filament axis, and z as the coordinate along the vortex filament axis; the shear layer boundary assumed to be locally straight and aligned along $\theta = 0, \pi$):

$$\frac{\partial v_r}{\partial t} + v_r \frac{\partial v_r}{\partial r} + \frac{v_\theta}{r} \frac{\partial v_r}{\partial \theta} + v_z \frac{\partial v_r}{\partial z} - \frac{v_\theta^2}{r} = F + v \left(\nabla^2 v_r - \frac{v_r}{r^2} - \frac{2}{r^2} \frac{\partial v_\theta}{\partial \theta} \right) \quad (\text{A1a})$$

$$F = -\frac{1}{\rho} \frac{\partial P}{\partial r} + g_r + \frac{1}{\rho} \frac{\partial}{\partial r} \{ I [\delta(\theta) + \delta(\theta - \pi)] \} \quad (\text{A1b})$$

An impulsive force term has been incorporated into the r-momentum Navier-Stokes equation, equations A1a–b, as a “driving” force that results from vortex flow crossing the slipstream boundary. $I(\delta(\theta) + \delta(\theta - \pi))$ is an impulsive force function where $\delta(\theta)$ and $\delta(\theta - \pi)$ are Dirac functions (e.g., ref. 15). (In short, $\delta(x - x_o) = 0$ for $x \neq x_o$ and $\delta(x - x_o) = \infty$ for $x = x_o$; finally, $\int_{-\infty}^{\infty} \delta(x - x_o) dx = 1$.) The impulsive force accounts for the net radial momentum change that occurs as vortex-driven flow crosses a prescribed, time-invariant, and discontinuous shear layer. (A “free” shear layer, on the other hand, would not remain discontinuous for large periods of time under the influence of viscosity (see ref. 6).) Refer to figures 2a–c. An expression for the vortex/shear layer impulsive force function, $I(\delta(\theta) + \delta(\theta - \pi))$, will be defined later in this appendix.

It is assumed that the decay of a vortex filament embedded in a shear layer is primarily a potential flow phenomenon. Additionally, the flow is assumed quasi-two-dimensional such that

$$\frac{\partial v_r}{\partial z} = \frac{\partial v_\theta}{\partial z} = 0 \quad \text{for all } \theta$$

but

$$\frac{\partial v_z}{\partial z} = 0 \quad \text{for } \theta \neq n\pi \text{ where } n = 0, 1, 2, \dots$$

$$\frac{\partial v_z}{\partial z} = \frac{\partial v_z}{\partial t} \frac{\partial t}{\partial z} = \frac{1}{v_z} \frac{\partial v_z}{\partial t} \neq 0 \quad \text{for } \theta = n\pi \text{ where } n = 0, 1, 2, \dots$$

Continuity would suggest for this quasi-two-dimensional flow that

$$\frac{\partial v_\theta}{\partial \theta} \propto \delta(\theta - n\pi) \quad \text{for } \theta = n\pi$$

Therefore, invoking the inviscid, quasi-two-dimensional flow assumptions reduces equations A1a–b to

$$\frac{\partial v_r}{\partial t} + v_r \frac{\partial v_r}{\partial r} + \frac{v_\theta}{r} \frac{\partial v_r}{\partial \theta} - \frac{v_\theta^2}{r} = F \quad (A2)$$

Finally, it is assumed that, for vortex dominated flows, the following approximation can be made:

$$\frac{v_\theta^2}{r} \approx \frac{1}{\rho} \frac{\partial P}{\partial r}$$

The above is only strictly true for steady vortex flow fields and, therefore, inherent in this approximation is the assumption that the vortex core contraction/expansion rate is small in magnitude. Proceeding with this approximation

$$\frac{\partial v_r}{\partial t} + v_r \frac{\partial v_r}{\partial r} + \frac{v_\theta}{r} \frac{\partial v_r}{\partial \theta} \approx \frac{1}{\rho} \frac{\partial}{\partial r} \{I[\delta(\theta) + \delta(\theta - \pi)]\} \quad (A3)$$

Integration of equation A3 with respect to the angular coordinate, θ , transforms the impulsive force to an incremental momentum change across the slipstream boundary (see ref. 15). This integral operation against equation A3 is performed, drawing upon an analogy from applied mechanics as to the mathematical treatment of impulsive forces in classic dynamic system analysis. Integration of an impulsive function over the complete domain of the function's independent variable yields a finite, net momentum change. In classic dynamic problems, the impulse function independent variable is time and the function integrated across zero to infinity yields the dynamic system's net momentum change. In the case of a vortex interaction with the slipstream shear layer, the impulse function's independent variable is θ and so integrating from $0 < \theta < 2\pi$ yields the total net momentum change for a unit volume of vortical flow as it crosses the slipstream boundary twice in one revolution.

$$\frac{\partial}{\partial t} \left(\int v_r d\theta \right) + \int \left\{ v_r \frac{\partial v_r}{\partial r} + \frac{v_\theta}{r} \frac{\partial v_r}{\partial \theta} \right\} d\theta \approx \frac{1}{\rho} \frac{\partial}{\partial r} \left\{ \int I[\delta(\theta) + \delta(\theta - \pi)] d\theta \right\} \quad (A4)$$

Or, making the substitution for the incremental momentum change, i.e.,

$$\frac{1}{\rho} \frac{\partial}{\partial r} \left\{ \int I[\delta(\theta) + \delta(\theta - \pi)] d\theta \right\} = -2v_i \frac{\partial v_\theta}{\partial r} \Big|_{\theta=0,\pi}$$

yields

$$\frac{\partial}{\partial t} \left(\int_0^{2\pi} v_r d\theta \right) + \int_0^{2\pi} \left\{ v_r \frac{\partial v_r}{\partial r} + \frac{v_\theta}{r} \frac{\partial v_r}{\partial \theta} \right\} d\theta \approx -2v_i \frac{\partial v_\theta}{\partial r} \Big|_{\theta=0,\pi} \quad (A5)$$

where the term $\partial v_\theta / \partial r|_{\theta=0,\pi}$ denotes the derivative of the tangential velocity with respect to the radial coordinate as evaluated at either $\theta = 0$ or π , as the derivatives at these two polar coordinates are equal in magnitude and sign. Therefore, in interpreting equation A5, it should be noted that as a unit volume of vortical flow crosses the slipstream boundary the flow sees an impulsive step in radial velocity of v_i , towards the core center.

Solution for a Rankine Vortex

In order to proceed with the analysis it is now necessary to assume a general expression for the stream function that is based, in part, on unknown functions that will later be solved for. It is assumed that there are three major components to the stream function for the flow region defined by $\theta \neq n\pi$, where $n = 0, 1, 2, \dots$. A separate stream function term, Ψ_* , will be defined later for $\theta = n\pi$ to completely describe the quasi-two-dimensional flow regime. Letting

$$\Psi = \Psi_{\text{Uniform Slipstream Flowfield}} + \Psi_{\text{Rankine Vortex Flowfield}} + \Psi_{\text{Vortex/Shear Layer Interaction}}$$

where

$$\Psi_{\text{Uniform Slipstream Flowfield}} = -\frac{1}{2} v_i \operatorname{sgn}(\theta - \pi) r \sin \theta$$

Note that if the above expression is transformed from polar coordinates to Cartesian coordinates, and the appropriate partial derivatives are taken to define the flowfield velocities (v_x and v_y versus v_r and v_θ), it can be shown, as expected, that

$$v_x = \frac{\partial \Psi_{\text{Uniform Slipstream Flowfield}}}{\partial y} = \begin{cases} +v_i/2 \\ -v_i/2 \end{cases} \text{ for } \begin{cases} y < 0 \\ y > 0 \end{cases}$$

$$v_y = -\frac{\partial \Psi_{\text{Uniform Slipstream Flowfield}}}{\partial x} = 0$$

and, further,

$$\Psi_{\text{Rankine Vortex Flowfield}} = \frac{\gamma}{4\pi} f(t) \left\{ \ln(r) [1 + \operatorname{sgn}(r - r_c)] + \frac{1}{2} \left(\frac{r}{r_c g(t)} \right)^2 [1 + \operatorname{sgn}(r_c - r)] \right\}$$

where, for $t = 0$, by definition, the unknown functions have the value $g(0) = f(0) = 1$. Therefore, for $t = 0$, the above expression reverts to the stream function—and correspondingly the velocities (v_r and v_θ)—of the classic analytical expressions for a Rankine vortex, i.e.,

$$\Psi_{\text{Rankine Vortex Flowfield}} = \begin{cases} \frac{\gamma}{4\pi} \left(\frac{r}{r_c} \right)^2 & r \leq r_c \\ \frac{\gamma}{2\pi} \ln(r) & r > r_c \end{cases} \quad \text{for } t = 0$$

$$v_\theta \equiv \frac{\partial \Psi_{\text{Rankine Vortex Flowfield}}}{\partial r} = \begin{cases} \frac{\gamma}{2\pi} \left(\frac{r}{r_c^2} \right) & r \leq r_c \\ \frac{\gamma}{2\pi} \left(\frac{1}{r} \right) & r > r_c \end{cases} \quad \text{for } t = 0$$

$$v_r = -\frac{1}{r} \frac{\partial \Psi_{\text{Rankine Vortex Flowfield}}}{\partial \theta} = 0$$

and, finally,

$$\Psi_{\text{Vortex/Shear Layer Interaction}} = h(t)\alpha(r)\chi(\theta)$$

which is comprised of the product of three unknown (but assumed separable) spatial and time-dependent functions.

Therefore, in summary, it is assumed that the stream function can be given by the expression

$$\begin{aligned} \Psi = & -\frac{1}{2} v_i \operatorname{sgn}(\theta - \pi) r \sin \theta + \frac{\gamma}{4\pi} f(t) \left\{ \ln(r) [1 + \operatorname{sgn}(r - r_c)] + \frac{1}{2} \left(\frac{r}{r_c g(t)} \right)^2 [1 + \operatorname{sgn}(r_c - r)] \right\} \\ & + h(t)\alpha(r)\chi(\theta) \end{aligned} \quad (\text{A6})$$

where

$$\text{Circulation} = \gamma f(t) \quad (\text{A7a})$$

$$\text{Core Radius} = r_c g(t) \quad (\text{A7b})$$

Equations A6 and A7a–b represent the superposition of a shear layer and a Rankine vortex (modified to incorporate time dependent functions for circulation and core radius) and the addition of a vortex/shear layer interaction term. See reference 16, for example, for additional discussion as to Rankine vortices. A Rankine vortex was selected to model this problem as it is a finite-core vortex model that inherently satisfies the steady-state potential flow equation. It is recognized that a Rankine vortex has substantial limitations as to its accuracy in modeling the velocity distributions of rotor trailed

tip vortices. Yet, for the purposes of this paper, which emphasizes deducing the first-order, time-dependent behavior of vortex core size and circulation, this should not pose a concern.

To accommodate the assumption of quasi-two-dimensional flow, the definition of velocity terms with respect to the stream function will be subtly modified:

$$v_r \equiv -\frac{1}{r} \frac{\partial \psi}{\partial \theta} \quad \text{but} \quad v_\theta \equiv \frac{\partial}{\partial r} (\psi + \psi_*) \quad (\text{A8a})$$

where

$$\psi_* = \varepsilon(t) \phi(r) p(\theta) \quad (\text{A8b})$$

$$p(\theta) \equiv b \text{Int} \left(\frac{\theta + \pi}{\pi} \right) \quad (\text{A8c})$$

Note that $p(\theta)$ is a variation on the step (“Heaviside”) function—except that the step is progressive with each crossing of the slipstream/shear layer boundary. $p(\theta)$ is a generalized function just as the step, signum, and the Dirac (“delta”) functions are (ref. 17). In accordance with the definition/assumption of quasi-two-dimensional flow, it can be seen that $\partial v_\theta / \partial \theta|_{\theta=n\pi} \propto \partial(p(\theta)) / \partial \theta$ where, as earlier hypothesized, $\partial(p(\theta)) / \partial \theta \propto \delta(\theta - n\pi)$. The coefficient b in equation A8c is a constant.

Therefore, the velocity functions that satisfy equation A6 must have the form:

$$v_r = \frac{1}{2} v_i \text{sgn}(\theta - \pi) \cos \theta - \frac{1}{r} h(t) \alpha(r) \frac{d}{d\theta} (\chi(\theta)) \quad (\text{A9a})$$

$$v_\theta = -\frac{1}{2} v_i \text{sgn}(\theta - \pi) \sin \theta + \frac{\gamma}{4\pi} f(t) \left\{ \left(\frac{1}{r} \right) [1 + \text{sgn}(r - r_c)] + \frac{r}{r_c^2 g(t)^2} [1 + \text{sgn}(r_c - r)] \right\} \\ + h(t) \chi(\theta) \frac{d}{dr} (\alpha(r)) + \varepsilon(t) p(\theta) \frac{d}{dr} (\phi(r)) \quad (\text{A9b})$$

where $\text{sgn}(x)$ is the signum function, and $\text{sgn}(x) = -1$ for $x < 0$, $\text{sgn}(x) = 0$ for $x = 0$, and $\text{sgn}(x) = +1$ for $x > 0$.

The signum and integer functions can be expressed in terms of unit step or Heaviside functions. Dirac (delta) functions, $\delta(x)$, have already been employed in the derivation of the governing equation, equation A5; Dirac functions will also manifest themselves in the evaluation of equation A5. The step and Dirac (delta) functions are “generalized” functions (see ref. 17). Formulas for integral and differential operations applied to generalized functions are well established.

The identification of analytical expressions for $f(t)$, $g(t)$, $h(t)$, $\alpha(r)$, $\chi(\theta)$, $\varepsilon(t)$, and $\phi(r)$ that satisfy equation A5 (shown immediately below, once again, for convenience) is the principal undertaking of this paper.

$$\frac{\partial}{\partial t} \left(\int_0^{2\pi} v_r d\theta \right) + \int_0^{2\pi} \left\{ v_r \frac{\partial v_r}{\partial r} + \frac{v_\theta}{r} \frac{\partial v_r}{\partial \theta} \right\} d\theta \approx -2v_i \frac{\partial v_\theta}{\partial r} \Big|_{\theta=0,\pi}$$

Substitution of equations A9a–b (the assumed functions for the radial and tangential velocities) into equation A5 yields the following results for the integro-differential terms in equation A5:

$$\begin{aligned} \frac{\partial}{\partial t} \left(\int_0^{2\pi} v_r d\theta \right) &= \frac{\partial}{\partial t} \left\{ \int_0^{2\pi} \left[\frac{1}{2} v_i \operatorname{sgn}(\theta - \pi) \cos \theta - \frac{1}{r} h(t) \alpha(r) \frac{d}{d\theta} (\chi(\theta)) \right] d\theta \right\} \\ &= -\frac{\alpha(r)}{r} \frac{d}{dt} (h(t)) \chi(\theta) \Big|_0^{2\pi} \end{aligned} \quad (\text{A10a})$$

$$\begin{aligned} \int_0^{2\pi} \left\{ v_r \frac{\partial v_r}{\partial r} \right\} d\theta &= - \int_0^{2\pi} \left\{ \frac{1}{2} v_i \operatorname{sgn}(\theta - \pi) \cos \theta - \frac{1}{r} h(t) \alpha(r) \frac{d}{d\theta} (\chi(\theta)) \right\} \left\{ h(t) \frac{\partial}{\partial r} \left(\frac{\alpha(r)}{r} \right) \frac{d}{d\theta} (\chi(\theta)) \right\} d\theta \\ &= -\frac{1}{2} v_i h(t) \frac{\partial}{\partial r} \left(\frac{\alpha(r)}{r} \right) \int_0^{2\pi} \left(\frac{d}{d\theta} (\chi(\theta)) \operatorname{sgn}(\theta - \pi) \cos \theta \right) d\theta \\ &\quad + h^2(t) \alpha(r) \frac{\partial}{\partial r} \left(\frac{\alpha(r)}{r} \right) \int_0^{2\pi} \left(\frac{d}{d\theta} (\chi(\theta)) \right)^2 d\theta \end{aligned} \quad (\text{A10b})$$

$$\begin{aligned}
& \int_0^{2\pi} \left\{ \frac{v_\theta}{r} \frac{\partial v_r}{\partial \theta} \right\} d\theta = \\
& \frac{\gamma}{4\pi} f(t) \left\{ \left(\frac{1}{r^2} \right) [1 + \text{sgn}(r - r_c)] + \frac{1}{r_c^2 g(t)^2} [1 + \text{sgn}(r_c - r)] \right\} \left\{ \frac{1}{2} v_i \text{sgn}(\theta - \pi) \cos \theta - \frac{1}{r} h(t) \alpha(r) \frac{d}{d\theta} (\chi(\theta)) \right\} \Big|_0^{2\pi} \\
& - \frac{1}{r} \int_0^{2\pi} \left\{ -\frac{1}{2} v_i \text{sgn}(\theta - \pi) \sin \theta + h(t) \chi(\theta) \frac{d}{dr} (\alpha(r)) + \varepsilon(t) p(\theta) \frac{d}{dr} (\varphi(r)) \right\} \left\{ \frac{1}{2} v_i \text{sgn}(\theta - \pi) \sin \theta \right\} d\theta \\
& + \frac{1}{r} \int_0^{2\pi} \left\{ -\frac{1}{2} v_i \text{sgn}(\theta - \pi) \sin \theta + h(t) \chi(\theta) \frac{d}{dr} (\alpha(r)) + \varepsilon(t) p(\theta) \frac{d}{dr} (\varphi(r)) \right\} \left\{ \frac{1}{2} v_i \frac{d}{d\theta} (\text{sgn}(\theta - \pi)) \cos \theta \right\} d\theta \\
& + \frac{1}{r} \int_0^{2\pi} \left\{ -\frac{1}{2} v_i \text{sgn}(\theta - \pi) \sin \theta + h(t) \chi(\theta) \frac{d}{dr} (\alpha(r)) + \varepsilon(t) p(\theta) \frac{d}{dr} (\varphi(r)) \right\} \left\{ -\frac{1}{r} h(t) \alpha(r) \frac{d^2}{d\theta^2} (\chi(\theta)) \right\} d\theta
\end{aligned} \tag{A10c}$$

$$\begin{aligned}
\left. \frac{\partial v_\theta}{\partial r} \right|_{\theta=0,\pi} &= \frac{\gamma}{4\pi} f(t) \left\{ \left(-\frac{1}{r^2} \right) [1 + \text{sgn}(r - r_c)] + \frac{1}{r_c^2 g(t)^2} [1 + \text{sgn}(r_c - r)] \right\} \\
&+ \left\{ h(t) \chi(\theta) \frac{d^2}{dr^2} (\alpha(r)) + \varepsilon(t) p(\theta) \frac{d^2}{dr^2} (\varphi(r)) \right\} \Big|_{\theta=0,\pi}
\end{aligned} \tag{A10d}$$

Flow visualization of rotor wakes—showing the interaction of the tip vortices with the slipstream—reveals spiral-like flow patterns (e.g., refs. 9 and 10). This leads to the insight that the vortex/slipstream interaction term in the stream function could perhaps be approximately represented by the simple analytic expression for a spiral, $\Psi_{\text{Vortex/Shear Layer Interaction}} \propto r\theta$.

Proceeding with this insight/hypothesis, it will be shown that equation A5 (for $r \geq r_c g(t)$) can be satisfied if the following functional forms for $\alpha(r)$, $\chi(\theta)$, and $\varphi(r)$ are employed:

$$\alpha(r) = ar \tag{A11a}$$

$$\chi(\theta) = c\theta \tag{A11b}$$

And, further, assume that

$$\varphi(r) = \alpha(r) = ar \tag{A11c}$$

$$\varepsilon(t) = h(t) \tag{A11d}$$

The assumptions explicit in equations A11c–d can be rationalized on the basis of functional analysis. Substituting the assumed functions, equations A11a–d, into equation A10a–d, for $\alpha(r)$, $\chi(\theta)$, $\varepsilon(t)$, and $\varphi(r)$, yields:

$$\frac{\partial}{\partial t} \left(\int_0^{2\pi} v_r d\theta \right) = -2\pi c a \frac{d}{dt} (h(t)) \quad (\text{A12a})$$

$$\int_0^{2\pi} \left\{ v_r \frac{\partial v_r}{\partial r} \right\} d\theta = 0 \quad (\text{A12b})$$

$$\begin{aligned} \int_0^{2\pi} \left\{ \frac{v_\theta}{r} \frac{\partial v_r}{\partial \theta} \right\} d\theta &= \frac{\gamma v_i}{2\pi} f(t) \left\{ \left(\frac{1}{r^2} \right) [1 + \text{sgn}(r - r_c)] + \frac{1}{r_c^2 g(t)^2} [1 + \text{sgn}(r_c - r)] \right\} \\ &\quad - \frac{1}{r} \int_0^{2\pi} \left\{ -\frac{1}{2} v_i \text{sgn}(\theta - \pi) \sin \theta + a h(t) (c\theta + p(\theta)) \right\} \left\{ \frac{1}{2} v_i \text{sgn}(\theta - \pi) \sin \theta \right\} d\theta \\ &\quad + \frac{1}{r} \int_0^{2\pi} \left\{ -\frac{1}{2} v_i \text{sgn}(\theta - \pi) \sin \theta + a h(t) (c\theta + p(\theta)) \right\} \left\{ \frac{1}{2} v_i \frac{d}{d\theta} (\text{sgn}(\theta - \pi)) \cos \theta \right\} d\theta \end{aligned} \quad (\text{A12c})$$

$$\left. \frac{\partial v_\theta}{\partial r} \right|_{\theta=0,\pi} = \frac{\gamma}{4\pi} f(t) \left\{ \left(-\frac{1}{r^2} \right) [1 + \text{sgn}(r - r_c)] + \frac{1}{r_c^2 g(t)^2} [1 + \text{sgn}(r_c - r)] \right\} \quad (\text{A12d})$$

Equations A12a–d can be further reduced by noting the following identities (ref. 17):

$$\frac{d}{d\theta} (\text{sgn}(\theta - \pi)) = 2\delta(\theta - \pi) \quad (\text{A13a})$$

$$\int_{-\infty}^{\infty} f(x) \delta(x - x_o) dx = f(x_o) \quad (\text{A13b})$$

This is the well-known “sampling property” of the Dirac (delta) function. $f(x)$ is any continuous function.

$$\int_{-\infty}^{\infty} f(x) u(x - x_o) \delta(x - x_o) dx = \int_{-\infty}^{\infty} f(x) k \delta(x - x_o) dx = k f(x_o) \quad (\text{A13c})$$

Where $u(x - x_o)$, as used in the above equation, is the unit step function, $f(x)$ is any continuous function, and k is a constant (where $0 \leq k \leq 1$). Various authors assign several different values to k but the value used by the majority, and adopted in this paper, is $k = 1/2$.

$$\int_0^{2\pi} \text{sgn}(\theta - \pi) \sin \theta d\theta = -4 \quad (\text{A13d})$$

$$\int_0^{2\pi} [\text{sgn}(\theta - \pi) \sin \theta]^2 d\theta = \int_0^{2\pi} \sin^2 \theta d\theta = \pi \quad (\text{A13e})$$

$$\int_0^{2\pi} \text{sgn}(\theta - \pi) \theta \sin \theta d\theta = -4\pi \quad (\text{A13f})$$

$$\int_0^{2\pi} \text{Int}\left(\frac{\theta + \pi}{\pi}\right) \text{sgn}(\theta - \pi) \sin \theta d\theta = -6 \quad (\text{A13g})$$

Applying equations A13a–g to equations A12a–d gives

$$\frac{\partial}{\partial t} \left(\int_0^{2\pi} v_r d\theta \right) = -2\pi c a \frac{d}{dt} (h(t)) \quad (\text{A14a})$$

$$\int_0^{2\pi} \left\{ v_r \frac{\partial v_r}{\partial r} \right\} d\theta = 0 \quad (\text{A14b})$$

$$\begin{aligned} \int_0^{2\pi} \left\{ \frac{v_\theta}{r} \frac{\partial v_r}{\partial \theta} \right\} d\theta = & + \frac{\gamma v_i}{2\pi} f(t) \left\{ \left(\frac{1}{r^2} \right) [1 + \text{sgn}(r - r_c)] + \frac{1}{r_c^2 g(t)^2} [1 + \text{sgn}(r_c - r)] \right\} \\ & + \frac{\pi}{r} \left(\frac{v_i}{2} \right)^2 + (\pi c + 2b) \frac{a h(t)}{r} v_i \end{aligned} \quad (\text{A14c})$$

$$\left. \frac{\partial v_\theta}{\partial r} \right|_{\theta=0, \pi} = \frac{\gamma}{4\pi} f(t) \left\{ \left(-\frac{1}{r^2} \right) [1 + \text{sgn}(r - r_c)] + \frac{1}{r_c^2 g(t)^2} [1 + \text{sgn}(r_c - r)] \right\} \quad (\text{A14d})$$

The constant b, in the function p(θ), can be determined by taking into account symmetry considerations for the vortex interaction, i.e.,

$$v_\theta|_{\theta=\pi^+} = v_\theta|_{\theta=0^+} \quad (\text{A15})$$

which gives (making the appropriate substitutions from eq. A9a into eq. A15)

$$b = -\pi c \quad (\text{A16})$$

Substituting the integro-differential terms of equations A14a–d back into equation A5 gives

$$-2\pi ac \frac{d}{dt}(h(t)) + \frac{\pi}{4r} v_i^2 - \frac{\pi ac v_i}{r} h(t) = -\frac{\gamma v_i}{2\pi r_c^2 g(t)^2} [1 + \text{sgn}(r_c - r)] \quad (\text{A17})$$

Equation A17 can only hold true for $r \geq r_c g(t)$. Therefore,

$$-2\pi ac \frac{d}{dt}(h(t)) + \frac{\pi}{4r} v_i^2 - \frac{\pi ac v_i}{r} h(t) = 0 \quad (\text{A18})$$

Equation A18 then requires that

$$\frac{d}{dt}(h(t)) = 0$$

or, more specifically,

$$h(t) = \frac{v_i}{4ac} \quad (\text{A19})$$

Equation A19 will only be valid until such time as the vortex completely decays out. Once the vortex decays out then $h(t) = 0$.

To recap, the stream function that satisfies the r-momentum equation for a Rankine vortex embedded on a slipstream shear layer has been found to be (for $r \geq r_c g(t)$)

$$\psi = -\frac{1}{2} v_i \text{sgn}(\theta - \pi) r \sin \theta + \frac{\gamma}{4\pi} f(t) \left\{ \ln(r) [1 + \text{sgn}(r - r_c)] + \frac{1}{2} \left(\frac{r}{r_c g(t)} \right)^2 [1 + \text{sgn}(r_c - r)] \right\} + kr\theta \quad (\text{A20a})$$

where k , a constant, is given by

$$k = \frac{v_i}{4} \quad (\text{A20b})$$

and

$$\psi_* = -\pi kr \text{Int} \left(\frac{\theta + \pi}{\pi} \right) \quad (\text{A20c})$$

The positive sign of the constant, k , is consistent with the inward (towards the vortex core) radial velocity that the impulsive force imparts across the shear layer. Given equations A9a–b, A16, and A20a–b, the velocities v_θ and v_r are therefore

$$v_r = \frac{1}{2} v_i \operatorname{sgn}(\theta - \pi) \cos \theta - k \quad (\text{A21a})$$

$$v_\theta = -\frac{1}{2} v_i \operatorname{sgn}(\theta - \pi) \sin \theta + \frac{\gamma}{4\pi} f(t) \left\{ \left(\frac{1}{r} \right) [1 + \operatorname{sgn}(r - r_c)] + \frac{r}{r_c^2 g(t)^2} [1 + \operatorname{sgn}(r_c - r)] \right\} \\ + k \left(\theta - \pi \operatorname{Int} \left(\frac{\theta + \pi}{\pi} \right) \right) \quad (\text{A21b})$$

Unfortunately, a solution for the stream function for the flow in the vortex core does not suggest itself at this time. This limitation in the analytical treatment of the vortex/slipstream problem does not adversely impact the evaluation of the vortex core size and circulation time dependence, as can be seen in appendix B.

Finally, it should be noted that there is an outer radial limit, r_o , for which the derived stream function applies. Beyond this limit there is no longer any mass transfer (via nonzero vortex tangential velocities) across the shear layer. This outer limit can be derived by noting that

$$v_\theta|_{\theta=0} = v_\theta|_{\theta=\pi} = 0 \quad \text{at} \quad r = r_o$$

which, given equation A21b, yields

$$\frac{\gamma}{2\pi} \frac{f(t)}{r_o} - \pi k = 0$$

Therefore

$$r_o = \frac{\gamma}{2\pi^2 k} f(t) \quad (\text{A22})$$

In conclusion, equations A20–A21, inclusive, are valid for the region defined by the radial limits

$$r_c g(t) \leq r < \frac{\gamma}{2\pi^2 k} f(t)$$

APPENDIX B – VORTEX CORE SIZE AND CIRCULATION TIME DEPENDENCE

Next, this paper will concentrate on deriving expressions for $f(t)$ and $g(t)$ for the stream function for $r \geq r_c$. It is possible to deduce the functional dependence of the vortex core size with time by noting the following relation.

$$\left. \frac{\partial r}{\partial t} \right|_{r=r_c} = \frac{1}{\left(\frac{\partial \tilde{\psi}}{\partial r} \right)} \cdot \left. \frac{\partial \tilde{\psi}}{\partial t} \right|_{r=r_c} \quad (\text{B1a})$$

where

$$\tilde{\psi} \equiv \int_0^{2\pi} (\psi + \psi_*) d\theta \quad (\text{B1b})$$

or, making the appropriate substitutions,

$$\tilde{\psi} = \frac{\gamma}{2} f(t) \left(\frac{r}{r_c g(t)} \right)^2 - \pi^2 k r$$

Refer to appendix A for the definitions of ψ and ψ_* . The expression for $\tilde{\psi}$ requires that equation B1a reduce to

$$\frac{\partial}{\partial t} f(t) = \left[4 \frac{f(t)}{g(t)} - \frac{2\pi^2 r_c k}{\gamma} \right] \frac{\partial}{\partial t} g(t)$$

Or, alternatively, using the chain rule for derivatives,

$$\frac{df}{dg} - 4 \left(\frac{f}{g} \right) + \frac{2\pi^2 r_c k}{\gamma} = 0 \quad (\text{B2})$$

The above is a homogeneous, linear ordinary differential equation which has the solution

$$f(t) = \left(\frac{2\pi^2 r_c k}{3\gamma} \right) g(t) + \left(1 - \frac{2\pi^2 r_c k}{3\gamma} \right) g(t)^4 \quad (\text{B3})$$

The initial value condition ($g(0) = f(0) = 1$) has been accounted for in equation B3.

To arrive at final closure for the functions $f(t)$ and $g(t)$, it is necessary to evaluate the vorticity conservation equation (ref. 18).

$$\frac{\partial}{\partial t} \left(\int \omega dV \right) = - \int (\omega \cdot n) u dS + \int (n \times F) dS \quad (B4a)$$

where

$$\omega = -\nabla^2 \psi \quad (B4b)$$

and

$$\nabla^2 \equiv \frac{\partial^2}{\partial r^2} + \frac{1}{r} \frac{\partial}{\partial r} + \frac{1}{r^2} \frac{\partial^2}{\partial \theta^2}$$

Note that $\nabla^2(\psi + \psi_*)$ and not $\nabla^2 \psi$ is used to defined the vorticity, but $\partial\psi/\partial\theta$ is used to define the vorticity convection velocity into the vortex control volume instead of $\partial(\psi + \psi_*)/\partial\theta$. Refer to appendix A, equations A20a–c, for the derivation of and expressions for ψ and ψ_* . The vorticity conservation equation, for a control volume about the vortex core, is reducible to (noting that there are no normal surface forces at the vortex core boundary):

$$\frac{\partial}{\partial t} \left\{ \int_0^{2\pi} \int_0^{r_c g(t)} \nabla^2(\psi + \psi_*) r dr d\theta \right\} = \int_0^{2\pi} \left\{ \frac{\partial\psi}{\partial\theta} + r_c^2 \frac{d}{dt} g(t) \right\} \nabla^2(\psi + \psi_*) d\theta \bigg|_{r=r_c} \quad (B5)$$

The vorticity convection into the vortex core, due to the shear-layer-induced radial flow, has to take into account the vortex core contraction/expansion rate. The vortex core contraction/expansion rate expression is $r_c \frac{d}{dt} g(t)$ and has been included in equation B5.

Given equations A20a–c and A21a–b, the vorticity can be defined by noting that

$$\nabla^2(\psi + \psi_*) = \frac{1}{r} k \left\{ \theta - \pi \text{Int} \left(\frac{\theta + \pi}{\pi} \right) \right\} - \frac{\pi k}{r} \delta'(\theta - \pi) - \frac{v_i}{r} \{ 2\delta(\theta - \pi) \cos \theta + \delta'(\theta - \pi) \sin \theta \} \quad \text{for } r \geq r_c g(t) \quad (B6)$$

In the above nomenclature $\delta'(x) = d(\delta(x))/dx$. Making the substitution of equation B6 into B5 and noting the following three points: (1) the control volume boundary is a function of time; (2) only the vorticity generated by the vortex/shear layer interaction for $r \geq r_c g(t)$ is convected into the control

volume; and (3) $\int_0^{2\pi} \int_0^{r_c g(t)} \nabla^2 \psi r dr d\theta = \gamma f(t)$ for the vorticity contained in the vortex core. Therefore

$$\begin{aligned}
\gamma \frac{d}{dt} f(t) = & k \int_0^{2\pi} \left\{ \theta - \pi \text{Int}\left(\frac{\theta + \pi}{\pi}\right) - \pi \delta'(\theta - \pi) \right\} \left\{ -\frac{1}{2} v_i \text{sgn}(\theta - \pi) \cos \theta + k + r_c \frac{d}{dt} g(t) \right\} d\theta \\
& - v_i \int_0^{2\pi} \left\{ [2\delta(\theta - \pi) \cos \theta + \delta'(\theta - \pi) \sin \theta] \right\} \left\{ -\frac{1}{2} v_i \text{sgn}(\theta - \pi) \cos \theta + k + r_c \frac{d}{dt} g(t) \right\} d\theta
\end{aligned} \tag{B7}$$

The following integral relations are applicable in evaluating equation B7

$$\int_{-\infty}^{\infty} f(x) \delta'(x - x_o) dx = -f'(x_o) \tag{B8a}$$

$$\int_{-\infty}^{\infty} f(x) u(x - x_o) \delta'(x - x_o) dx = \int_{-\infty}^{\infty} f(x) k \delta'(x - x_o) dx = -k f'(x_o) \tag{B8b}$$

where $u(x - x_o)$, as used in the above equation, is the unit step function; $f'(x)$ is the derivative of a continuous function, $f(x)$, which in itself is also continuous; and k is a constant (where k is arbitrary in value).

Therefore, application of equations B8a–b to equation B7 results in a first-order, linear differential equation with the two unknown functions, $f(t)$ and $g(t)$

$$\gamma \frac{d}{dt} f(t) + \left(2v_i + \pi^2 r_c \frac{d}{dt} g(t) \right) k + \pi^2 k^2 = 0 \tag{B9}$$

Integrating equation B9 with respect to time yields

$$\gamma f(t) + \pi^2 k r_c g(t) = \pi^2 k r_c + \gamma - (2v_i k + \pi^2 k^2) t \tag{B10}$$

An initial value constraint of $g(0) = f(0) = 1$ has been accounted for in equation B10 by solving for the integration constant. The above equation is a nonlinear implicit solution for the vortex core size. The vortex core radius can readily be seen to decrease with time by noting an approximation for $g(t)$ at very large units of time when $f(t)$ and, therefore, the circulation approaches zero.

$$g(t) \approx 1 + \frac{\gamma}{\pi^2 k r_c} - \left(\frac{2v_i k + \pi^2 k^2}{\pi^2 k r_c} \right) t \tag{B11a}$$

as

$$t \rightarrow \frac{\pi^2 k r_c + \gamma}{2v_i k + \pi^2 k^2} \tag{B11b}$$

The interdependence of the initial value of circulation and the slipstream inflow velocity for rotor wakes can be found by simple momentum/vortex theory for rotors. The trailed circulation for a tip vortex filament shed in rotor axial flow can be found by the expression (see ref. 8):

$$\gamma = \frac{4\pi R v}{N V_T} (U + v) \quad (\text{B12})$$

where N is the number of blades and V_T is the rotor tip speed. The mean inflow at the rotor disk, v , is

$$v = -\frac{U}{2} + \sqrt{\left(\frac{U}{2}\right)^2 + \frac{C_T}{2} V_T^2} \quad (\text{B13})$$

As this analysis is applicable for the mid- to far-wake for rotors (i.e., the flow is steady, nonaccelerating), then based on simple momentum theory for rotors

$$v_i = 2v \quad (\text{B14})$$

To conclude this discussion an expression for the wake age required to completely collapse the vortex will be derived. Referring to equation B11b

$$\Delta\psi_w \equiv \Omega t = \Omega \frac{\pi^2 k r_c + \gamma}{2v_i k + \pi^2 k^2} \quad (\text{B15})$$

Making appropriate substitutions from equations B12, B13, and B14 into equation B15 yields

$$\Delta\psi_w = \left(\frac{\pi^2 + 8}{4} \right) \left(\frac{\Omega r_c}{v} \right) + \left(\frac{2\pi^2 + 16}{\pi N} \right) \left(1 + \frac{U}{v} \right) \quad (\text{B16})$$

APPENDIX C – VORTEX FILAMENT AXIAL FLOW

Axial Flow Along Slipstream Boundary for $t \ll \Delta\psi_w/\Omega$

The vortex/shear layer interaction problem has been assumed to be quasi-two-dimensional. This has been defined to be

$$\frac{\partial v_z}{\partial z} = 0 \quad \text{for } \theta \neq n\pi \quad \text{where } n = 0, 1, 2, \dots$$

but

$$\frac{\partial v_z}{\partial z} = \frac{\partial v_z}{\partial t} \frac{\partial t}{\partial z} = \frac{1}{v_z} \frac{\partial v_z}{\partial t} \neq 0 \quad \text{for } \theta = n\pi$$

The continuity equation along the shear layer/slipstream boundary can be rewritten as

$$\frac{1}{v_z} \frac{\partial v_z}{\partial t} = - \left\{ \frac{\partial v_r}{\partial r} + \frac{v_r}{r} + \frac{1}{r} \frac{\partial v_\theta}{\partial \theta} \right\} \quad (C1)$$

which gives

$$v_z = e^{-\int \left\{ \frac{\partial v_r}{\partial r} + \frac{v_r}{r} + \frac{1}{r} \frac{\partial v_\theta}{\partial \theta} \right\} dt} \quad (C2)$$

Finally, expressions for v_r and v_θ have been derived in appendix A and are given by equations 9 and 10 in the main body of the paper. Making the appropriate substitutions

$$v_z = e^{\pi k \delta (\theta - n\pi) t / r} \quad (C3)$$

Equation C3 predicts that v_z is a constant for $r < r_0$ (refer to appendix A, eq. A22, for the definition/derivation of r_0) for all θ —except along the slipstream boundary, i.e., $\theta = n\pi$. For $\theta = n\pi$, equation C3 describes a line-sink; some of the tangential mass flow crossing the slipstream boundary is redirected and convected axially along the shear layer. Continuity has, therefore, been shown to be preserved even at the discontinuous slipstream boundary (if one overcomes the conceptual hurdle of an infinite axial velocity, acting along an infinitesimal shear layer thickness, that increases with time). Equation C3 should be seen as a limiting case for more realistic shear layer models (shear layer gradients that are steep but not discontinuous). Therefore, axial velocities for actual rotor trailed tip vortices are large but finite, are concentrated at the slipstream boundary as “swirl,” and increase with time. Equation C3 provides an insight into observations of a large particle void seen in smoke flow visualization studies of rotor vortex filaments in that a finite axial flow is predicted for the remainder of the region $r < r_0$.

Axial Flow Along Slipstream Boundary for $t \rightarrow \infty$

The angular momentum in rotor vortex filaments, as they decay, is transformed to axial (z coordinate) momentum. Turning to the Navier-Stokes momentum equation for v_z

$$\frac{\partial v_z}{\partial t} + v_r \frac{\partial v_z}{\partial r} + \frac{1}{r} v_\theta \frac{\partial v_z}{\partial \theta} + v_z \frac{\partial v_z}{\partial z} = -\frac{1}{\rho} \frac{\partial P}{\partial z} + \nu \nabla^2 v_z \quad (C4)$$

Now, as previously noted, and continuing to assume inviscid flow

$$\frac{\partial P}{\partial z} = 0 \quad \text{and} \quad \frac{\partial v_z}{\partial z} = \frac{1}{v_z} \frac{\partial v_z}{\partial t}$$

Therefore

$$2 \frac{\partial v_z}{\partial t} + \frac{1}{r} v_\theta \frac{\partial v_z}{\partial \theta} + v_r \frac{\partial v_z}{\partial r} = 0 \quad (C5)$$

An asymptotic solution will now be derived for time approaching infinity, i.e. $t \rightarrow \infty$. This asymptotic solution is applicable only for $r > r_c$.

Note that as the vortex core collapses, then

$$\frac{\partial v_z}{\partial t} \rightarrow 0$$

$$f(t) \rightarrow 0$$

and

$$k = 0 \quad \text{as} \quad t \rightarrow \infty$$

Therefore, it can be readily seen that

$$v_z \rightarrow A e^{-b\psi} \quad \text{as} \quad t \rightarrow \infty$$

where A and b are arbitrary constants. Also, as $t \rightarrow \infty$, then

$$\psi \rightarrow -\frac{1}{2} v_i \text{sgn}(\theta - \pi) r \sin \theta \quad (\text{as the vortex core collapses})$$

Therefore, the axial velocity distribution must approach

$$v_z \rightarrow A e^{\frac{b}{2} v_i \text{sgn}(\theta - \pi) r \sin \theta} \quad (C6)$$

for

$$t \rightarrow \infty$$

The constants in the asymptotic expression, equation C6, can be approximately determined as follows. First, the constant b can be arbitrarily selected (for reasons that will become clear shortly) to be $b = 2/v_i$. Having made that selection, then, a value for the constant A can be evaluated by noting that the kinetic energy of the rotor blade root vortex should be counterbalanced by the kinetic energy of the asymptotic filament axial velocities (equivalent to swirl velocity in rotor wake global coordinates versus the filament local coordinates). Therefore

$$\text{K.E. Blade Root Swirl} = \text{K.E. Asymptotic Filament/Slipstream Swirl} \quad (\text{C7a})$$

$$\int_0^{2\pi} \int_0^R \left[\frac{2v^2 \Omega r}{(\Omega r)^2 + v^2} \right]^2 r dr d\theta \approx 2A^2 \left(\frac{R}{2} \right)^2 \int_0^{2\pi} \int_0^\infty e^{-y} dy dx \quad (\text{C7b})$$

The expression for the blade-root swirl velocity, in the left side of equation C7b, is derived in reference 8 by means of the method of calculus of variation for an extended momentum theory for rotor induced power and thrust. The kinetic energy equivalence relationship as represented by equations C7a–b is only approximate as only the blade root swirl within the slipstream boundary is accounted for. Through the above auspicious choice of the constant b in equation C6, the kinetic energy integral for the filament asymptotic axial velocity has a closed form solution. Another choice of the constant b would not have resulted in a closed form solution.

Ignoring higher order terms as being negligible in the integration results, the following solution for the constant A is derived. (Note $V_T = \Omega R$.)

$$A \approx -2 \frac{v^2}{V_T} \sqrt{\ln(V_T^2 + v^2) - 2 \ln(v)} \quad (\text{C8})$$

REFERENCES

1. Gray, R. B.: Vortex Modeling for Rotor Aerodynamics—The 1991 Alexander A. Nikolsky Lecture. 47th Annual Forum of the American Helicopter Society, Phoenix, Ariz., May 1991.
2. Swanson, A.; and Light, J.: Shadowgraph Flow Visualization of Isolated Tiltrotor and Rotor/Wing Wakes. 48th Annual Forum of the American Helicopter Society, Washington, D.C., June 1992.
3. Leishman, J. G.; Baker, A.; and Coyne, A.: Measurements of Rotor Tip Vortices Using Three-Component Laser Doppler Velocimetry. American Helicopter Society Aeromechanics Conference, Fairfield County, Conn., October 1995.
4. Han, Y. O.; Leishman, J. G.; and Coyne, A. J.: On the Turbulent Structure of a Tip Vortex Generated by a Rotor. 52nd Annual Forum of the American Helicopter Society, Washington, D.C., June 4–6, 1996.
5. Baker, A. M.: Three-Component Laser Doppler Velocimeter Measurements of a Tip Vortex Generated by a One-Bladed Rotor. Masters of Science Thesis, University of Maryland, 1995.
6. Lamb, H.: Hydrodynamics, Sixth Edition. Dover Publications, New York, 1945.
7. Friedrichs, K. O.: Special Topics in Fluid Dynamics. Gordon & Breach, Science Publishers, New York, 1966.
8. Johnson, W.: Helicopter Theory. Princeton University Press, 1980.
9. Landgrebe, A. J.: The Wake Geometry of a Hovering Helicopter Rotor and Its Influence on Rotor Performance. 28th Annual Forum of the American Helicopter Society, Washington, D.C., May 1972.
10. Favier, D.; Ettaouil, A.; and Maresca C.: Numerical and Experimental Investigation of Isolated Propeller Wakes in Axial Flight. AIAA Journal of Aircraft, vol. 26, no. 9, September 1989.
11. Saffman, P. G.: Vortex Dynamics. Cambridge University Press, 1992.
12. Adams, G. N.; and Gilmore, D. C.: Some Observations of Vortex Core Structure. Canadian Aeronautics and Space Journal, June 1972.
13. Thompson, T. L.; Komerath, N. M.; and Gray, R. B.: Visualization and Measurement of the Tip Vortex Core of a Rotor Blade in Hover. AIAA Journal of Aircraft, vol. 25, no. 12, December 1988.

14. Hylin, E. C.; and McDonough, J. M.: Additive Turbulent Decomposition Applied to an Isolated Vortex in a Constant Shear Flow. Fourth International Symposium on Computational Fluid Dynamics, University of California, Davis, September 9–12, 1991.
15. Wylie, C. R.: Advanced Engineering Mathematics, Fourth Edition. McGraw-Hill, 1975.
16. Durand, W. F.: Aerodynamic Theory. 1934.
17. Hoskins, R. F.: Generalised Functions. Ellis Horwood, Ltd., Chichester, United Kingdom of Great Britain, 1979.
18. White, F. M.: Viscous Fluid Dynamics. McGraw-Hill, 1974.

REPORT DOCUMENTATION PAGE			Form Approved OMB No. 0704-0188	
Public reporting burden for this collection of information is estimated to average 1 hour per response, including the time for reviewing instructions, searching existing data sources, gathering and maintaining the data needed, and completing and reviewing the collection of information. Send comments regarding this burden estimate or any other aspect of this collection of information, including suggestions for reducing this burden, to Washington Headquarters Services, Directorate for Information Operations and Reports, 1215 Jefferson Davis Highway, Suite 1204, Arlington, VA 22202-4302, and to the Office of Management and Budget, Paperwork Reduction Project (0704-0188), Washington, DC 20503.				
1. AGENCY USE ONLY (Leave blank)		2. REPORT DATE January 1997		3. REPORT TYPE AND DATES COVERED Technical Memorandum
4. TITLE AND SUBTITLE Rotor Vortex Filaments: Living on the Slipstream's Edge			5. FUNDING NUMBERS 505-59-36	
6. AUTHOR(S) Larry A. Young				
7. PERFORMING ORGANIZATION NAME(S) AND ADDRESS(ES) Ames Research Center Moffett Field, CA 94035-1000			8. PERFORMING ORGANIZATION REPORT NUMBER A-975569	
9. SPONSORING/MONITORING AGENCY NAME(S) AND ADDRESS(ES) National Aeronautics and Space Administration Washington, DC 20546-0001			10. SPONSORING/MONITORING AGENCY REPORT NUMBER NASA TM-110431	
11. SUPPLEMENTARY NOTES Point of Contact: Larry A. Young, Ames Research Center, MS T12-B, Moffett Field, CA 94035-1000 (415) 604-4022				
12a. DISTRIBUTION/AVAILABILITY STATEMENT Unclassified — Unlimited Subject Category 02			12b. DISTRIBUTION CODE	
13. ABSTRACT (Maximum 200 words) The purpose of this paper is to gain a better understanding of rotor wake evolution in hover and axial flow by deriving an analytical solution for the time dependent behavior of vortex filament circulation and core size. This solution is applicable only for vortex filaments in the rotor far-wake. A primarily inviscid vortex/shear layer interaction (where the slipstream boundary is modeled as a shear layer) has been identified in this analytical treatment. This vortex/shear layer interaction results in decreasing vortex filament circulation and core size with time. The inviscid vortex/shear layer interaction is shown, in a first-order treatment, to be of greater magnitude than viscous diffusion effects. The rate of contraction, and ultimate collapse, of the vortex filament core is found to be directly proportional to the rotor inflow velocity. This new insight into vortex filament decay promises to help reconcile several disparate observations made in the literature and will, hopefully, promote new advances in theoretical modeling of rotor wakes.				
14. SUBJECT TERMS Rotors, Vortices, Shear layer			15. NUMBER OF PAGES 43	
			16. PRICE CODE A03	
17. SECURITY CLASSIFICATION OF REPORT Unclassified	18. SECURITY CLASSIFICATION OF THIS PAGE Unclassified	19. SECURITY CLASSIFICATION OF ABSTRACT	20. LIMITATION OF ABSTRACT	